Available online at www.sciencedirect.com
SCIENCE DIRECT®
Combustion and Flame 143 (2005) 491–506
Combustion and Flame
www.elsevier.com/locate/combustflame

Lifted methane–air jet flames in a vitiated coflow

R. Cabra [a,c], J.-Y. Chen [a,*], R.W. Dibble [a], A.N. Karpetis [b,d], R.S. Barlow [b]

[a] *Mechanical Engineering Department, University of California, Berkeley, CA 94720, USA*
[b] *Combustion Research Facility, Sandia National Laboratories, Livermore, CA 94550, USA*
[c] *Hamilton-Sundstrand Power Systems, 4400 Ruffin Road, P.O. Box 85757, San Diego, CA 92186-5757, USA*
[d] *Aerospace Engineering Department, Texas A&M University, College Station, TX 77843-3141, USA*

Received 25 February 2005; received in revised form 28 August 2005; accepted 31 August 2005

Available online 10 October 2005

Abstract

The present vitiated coflow flame consists of a lifted jet flame formed by a fuel jet issuing from a central nozzle into a large coaxial flow of hot combustion products from a lean premixed H_2/air flame. The fuel stream consists of CH_4 mixed with air. Detailed multiscalar point measurements from combined Raman–Rayleigh–LIF experiments are obtained for a single base-case condition. The experimental data are presented and then compared to numerical results from probability density function (PDF) calculations incorporating various mixing models. The experimental results reveal broadened bimodal distributions of reactive scalars when the probe volume is in the flame stabilization region. The bimodal distribution is attributed to fluctuation of the instantaneous lifted flame position relative to the probe volume. The PDF calculation using the modified Curl mixing model predicts well several but not all features of the instantaneous temperature and composition distributions, time-averaged scalar profiles, and conditional statistics from the multiscalar experiments. A complementary series of parametric experiments is used to determine the sensitivity of flame liftoff height to jet velocity, coflow velocity, and coflow temperature. The liftoff height is found to be approximately linearly related to each parameter within the ranges tested, and it is most sensitive to coflow temperature. The PDF model predictions for the corresponding conditions show that the sensitivity of flame liftoff height to jet velocity and coflow temperature is reasonably captured, while the sensitivity to coflow velocity is underpredicted.

Keywords: Laser spectroscopy; Multiscalar measurements; Computational modeling; Reactions in flames; Vitiated flow

1. Introduction

In practical combustion systems hot combustion products are often recirculated to enhance flame stability. Prediction of turbulent flames with complex recirculating flows can be a significant challenge for current combustion models. The vitiated coflow flame is a turbulent reacting flow within a hot environment but with a simplified geometry. It consists of a fuel jet issuing into a coflow of hot combustion products from a lean premixed flame. The coflow diameter is much larger than the central jet diameter. This large diameter isolates the central fuel jet from ambient air for a sufficiently long distance so that the computational problem may be cast as a two-stream flow. Therefore, the vitiated coflow burner allows detailed experimental and computational investigation of turbulent

* Corresponding author.
E-mail address: jychen@me.berkeley.edu (J.-Y. Chen).

0010-2180/$ – see front matter
doi:10.1016/j.combustflame.2005.08.019

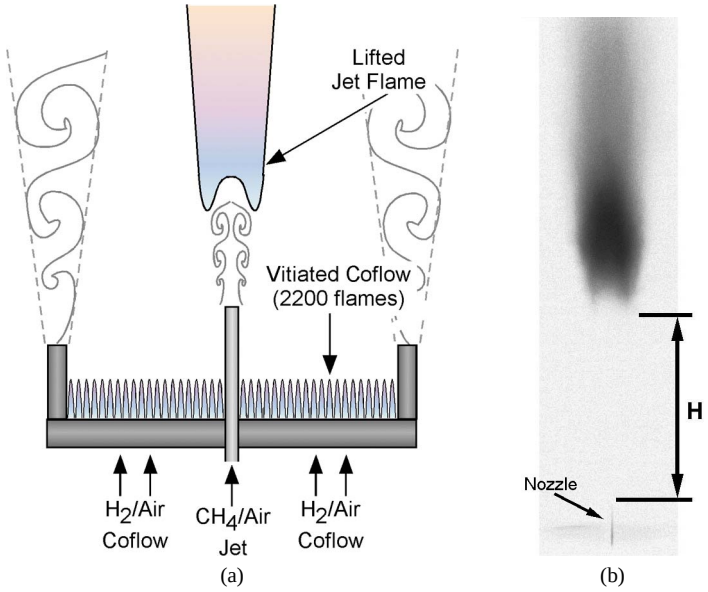

Fig. 1. (a) Burner schematic and (b) luminosity image (negative) of a lifted CH_4/air jet flame in vitiated coflow.

mixing and flame stabilization for a fuel flow in hot combustion products, while avoiding the additional complexities of recirculating fluid dynamics found in practical combustors or laboratory-scale swirl burners.

The present investigation of lifted CH_4/air jet flames is an extension of previous experimental and computational work on a lifted H_2/N_2 jet flame in vitiated coflow [1]. The H_2/N_2 and CH_4/air flames were selected to provide complementary experimental data to be used for evaluation of combustion models, with these methane cases following the kinetically simpler hydrogen case. As discussed in [1] and in recent computational studies of the H_2/N_2 case by Masri et al. [2] and Goldin [3], the vitiated coflow introduces autoignition as an additional possible mechanism of lifted flame stabilization. The liftoff height, which nominally corresponds to an average stabilization position of the flame, is sensitive to several flow and flame parameters, especially the coflow temperature as illustrated by a recent numerical study [4]. Therefore, the measured sensitivity of liftoff height to selected parameters is a useful basis for evaluation of combustion models, and this approach is used in the present work to test the probability density function (PDF) method of combustion modeling. Some features of the scalar structure of the H_2/N_2 flame are compared to those of the CH_4/air flame in the present paper.

Within PDF methods the mixing submodel remains an area in need of improvement (e.g., Pope [5] and Fox [6]). Past studies have examined the performance of available mixing models. For example, the modified Curl (M-Curl) mixing model [7] has performed well for turbulent jet flames of H_2 [8] and natural gas [9], as well as the H_2/N_2 lifted flame in vitiated coflow [1,2]. Subramaniam and Pope [10] found that the Euclidean Minimum Spanning Tree (EMST) model [11] outperformed the Interaction by Exchange with the Mean (IEM) model [11] for a flow with periodic reaction zones. Additionally, both the EMST [13] and the M-Curl [14] mixing models successfully predicted the piloted turbulent nonpremixed flames reported by Barlow and Frank [15]. The present study compares the performance of several mixing models in an environment that exhibits important similarities to practical combustor designs, in that there is mixing and flame stabilization of a turbulent fuel flow surrounded by lean combustion products. The CH_4/air jet flame is modeled by the joint scalar PDF approach using a series of mixing models, and experimental results are used to evaluate their relative performance.

2. Experimental methods

The vitiated coflow burner is shown schematically in Fig. 1a. The vitiated coflow was produced using a perforated plate (brass, 210-mm diameter and 12.7-mm thickness) as a premixed flame holder. A flow blockage of 87% was achieved by drilling 2200 holes (1.58-mm diameter) through the plate. Premixed H_2/air jet flames were stabilized on each hole, and their products mixed to form the vitiated coflow. An exit collar surrounded the coflow and served as a barrier that delayed entrainment of ambi-

ent air into the coflow region. Water flowing through a copper coil cooled the stainless-steel exit collar. The main jet flowed from a stainless-steel tube (6.35 mm o.d./4.57 mm i.d.), which extended 70 mm beyond the perforated plate surface. As will be shown below, measured profiles of temperature and species are uniform across this hot coflow, and the flow field of interest is unaffected by mixing with the ambient air. This allows the flames to be treated computationally as two-stream problems.

Multiscalar point measurements were performed in the Turbulent Diffusion Flame (TDF) laboratory at Sandia National Laboratories. Temperature and major species concentrations were measured simultaneously in a single-point fashion, using a Raman–Rayleigh scattering system. Two-photon laser-induced fluorescence (LIF) was used for the measurement of CO with accuracy better than was obtainable from the Raman technique. A separate LIF system was used for the determination of OH radical mass fractions in the flame. The spatial resolution of the combined measurements was 0.75 mm, which corresponds to the length along the laser axis that was imaged onto each detection system.

The separate pulsed laser systems were fired within an interval of less than 1 μs. At the highest flow velocity (∼100 m/s near the jet exit) this time interval corresponds to a convective length scale of 100 μm. Since this is small compared to the spatial resolution of the multiscalar system, the combined measurements can be considered instantaneous. The precision and accuracy of the Raman–Rayleigh–LIF system is determined via a series of measurements in flat calibration flames [16]. The measurement precision was determined from the standard deviations of these flat flame measurements: temperature, 1%; N_2, 3%; H_2O, 5%; CO_2, 6%; OH, 10%; and mixture fraction, 6%. Detailed documentation of diagnostic methods, system design, and system uncertainties may be found in the literature [15–19].

Visible chemiluminescence was used as the flame-front indicator, and the liftoff height was measured with a simple digital imaging system. A digital camera (Sony MVC-FD85), with a 1.3 megapixel resolution was mounted on a stand, and its spatial field of view was calibrated with a target before and after each set of experiments. A long exposure time (1 s at $f/2$) was necessary to capture the faint flame chemiluminescence. For each flame condition 10 to 20 digital images were averaged. An example of an averaged image is shown in Fig. 1b. The flame liftoff height was determined as the lowest point where luminosity from the flame was detected. This definition of the flame position is expected to underestimate of the average liftoff height and yield a result closer to the upstream end of the flame stabilization region. However, it provides a consistent measure for evaluating the sensitivity of liftoff height to changes in flow parameters.

Table 1
Base-case conditions for the vitiated coflow burner

	Hydrogen		Methane	
	Jet	Coflow	Jet	Coflow
Re	23,600	18,600	28,000	23,300
d (mm)	4.57	210	4.57	210
V (m/s)	107	3.5	100	5.4
T (K)	305	1,045	320	1,350
X_{O_2}	0.0021	0.15	0.15	0.12
X_{N_2}	0.74	0.75	0.52	0.73
X_{H_2O}	0.0015	0.099	0.0029	0.15
X_{OH} (ppm)	<1	<1	<1	200
X_{H_2}	0.25	5×10^{-4}	100	100
X_{NO} (ppm)	–	–	<1	<1
X_{CH_4}	–	–	0.33	0.0003
ϕ	–	0.25	–	0.4
f_s	0.473		0.177	

Conditions for both the hydrogen (previous work [1]) and the methane cases (present work) are listed. X, mole fraction; Re, Reynolds number; D, diameter; ϕ, equivalence ratio; f_s, stoichiometric mixture fraction.

3. Base-case flame: CH_4/air jet into vitiated coflow

Multiscalar point measurements were obtained for a single flame (base case), having a fuel jet mixture of 33% CH_4 and 67% air, by volume. Use of air rather than nitrogen makes a smaller flame and allows for higher Reynolds number flows before blowing off the flame. The bulk velocity of the fuel jet was $V_{jet} = 100$ m/s. The coflow consisted of products from a lean premixed H_2/air flame ($\phi = 0.40$) with a velocity of $V_{coflow} = 5.4$ m/s, which was determined from measured flow rates and the equilibrium composition at the measured coflow temperature. Details of experimental conditions are listed in Table 1. The liftoff height for the base-case condition was $H/d \cong 35$, determined visually. Measurements included a centerline profile extending from $z/d = 1$ to $z/d = 100$ downstream of the nozzle exit and radial profiles at several axial stations ($z/d = 1$, 15, 30, 40, 50, and 70). The radial extent covered by these profiles was from −3 to 50 mm, with a typical spacing of 2 or 3 mm. On average, 400 samples (laser shots) were collected at each location.

The instantaneous temperature and composition data were processed and the Favre averages and standard deviations were generated. For all comparisons, the mixture fraction formulated by Bilger et al. [20]

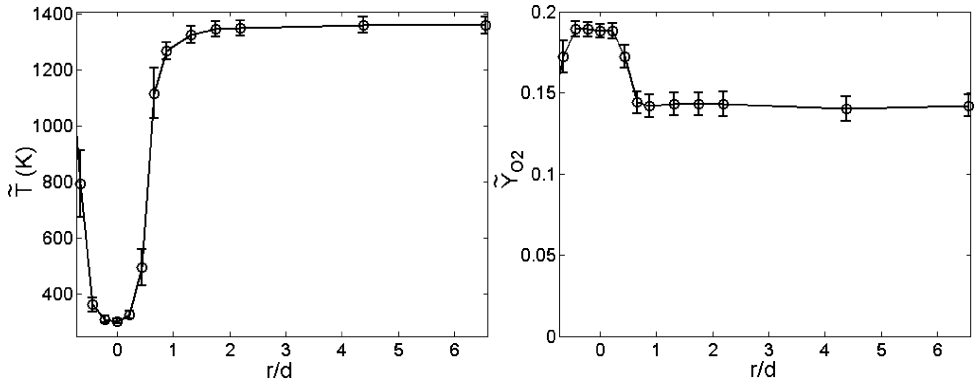

Fig. 2. Radial profiles of the Favre-averaged temperature and O_2 mass fraction at $z/d = 1$ for the CH_4/air jet flame into a vitiated coflow. Error bars denote the measured standard deviations.

was used:

$$f = \frac{2(Y_C - Y_{C,2})/M_C + (Y_H - Y_{H,2})/2M_H - (Y_O - Y_{O,2})/M_O}{2(Y_{C,1} - Y_{C,2})/M_C + (Y_{H,1} - Y_{H,2})/2M_H - (Y_{O,1} - Y_{O,2})/M_O}. \quad (1)$$

The elemental masses, M, and mass fractions, Y, of carbon, hydrogen, and oxygen, along with the boundary conditions established at the fuel (subscript 1) and coflow (subscript 2) streams, determine the mixture fraction. For the base-case conditions listed in Table 1, the stoichiometric mixture fraction was $f_s = 0.17$.

Two features of the experimental results serve to simplify the computational problem for this flame. First, radial profiles of temperature and oxygen mass fraction at $z/d = 1$ (Fig. 2) exhibit uniform scalar conditions in the jet and coflow, with fluctuation levels comparable to the precision of the measurement system. The radial profiles measured farther downstream (and presented in a later section) demonstrate that there is no mixing of ambient air into the region of the developing jet until well downstream of the flame stabilization region. This allows the flame to be modeled as a two-stream problem. Second, analysis of the single-shot multiscalar data at $z/d = 40$ and 50 confirmed that elemental mixture fractions based on carbon and hydrogen are in close agreement, meaning that differential diffusion effects are negligible in this flame, and the computational assumption of unity Lewis number is appropriate.

3.1. Comparison between CH_4/air and H_2/N_2 vitiated coflow flames

Figs. 3 and 4 present the scatter data from measurements of temperature and OH mass fraction obtained in the CH_4/air and H_2/N_2 flames [1], respectively. The estimated Damköhler numbers are order of unity at the locations where flames stabilize. Each of the data ensembles plotted in these figures was formed by combining single-point measurements along the whole radial profile at each axial location. This manner of presentation, namely scattered data of a reactive scalar such as temperature T against mixture fraction f, examines the scalar structure of the flame and provides a qualitative representation of the joint distribution function of the selected scalars. The experimental joint distributions of Fig. 3 exhibit a transition from a nonreacting flow (pure mixing) to a reacting flow. At $z/d = 30$, nearly all the instantaneous temperatures (left column) lie along the nonreacting solution, which is labeled as the dashed "Pure Mixing" line in the figure. Far downstream at $z/d = 70$, the measured temperatures are seen to move close to the equilibrium limit, marked by the solid gray line in each graph. A similar transition is seen in the distributions for OH (right column), and it is evident from these scatter data that the flame position fluctuates widely within the stabilization region from $z/d = 30$ to at least $z/d = 40$ and possibly beyond $z/d = 50$. The temperature and OH results both show a relaxation of reacted samples toward the equilibrium curves as we move downstream from $z/d = 40$ to $z/d = 70$. This reflects decreasing strain and increasing residence time as downstream distance increases. Note that there are a few temperature data points at $z/d = 70$ that correspond to mixing of ambient air into the coflow. These events are clearly rare and are considered unimportant for the calculation of these lifted flames.

Corresponding results for temperature and OH from the H_2/N_2 lifted flame [1] are shown in Fig. 4. Within their respective stabilization regions, both flames exhibit broadened distributions between the limits of pure mixing and full equilibrium, as do previous Raman spectroscopy measurements in lifted flames [21,22]. However, there are important differences between the CH_4/air and H_2/N_2 cases. The distributions of temperature and Y_{OH} in the methane

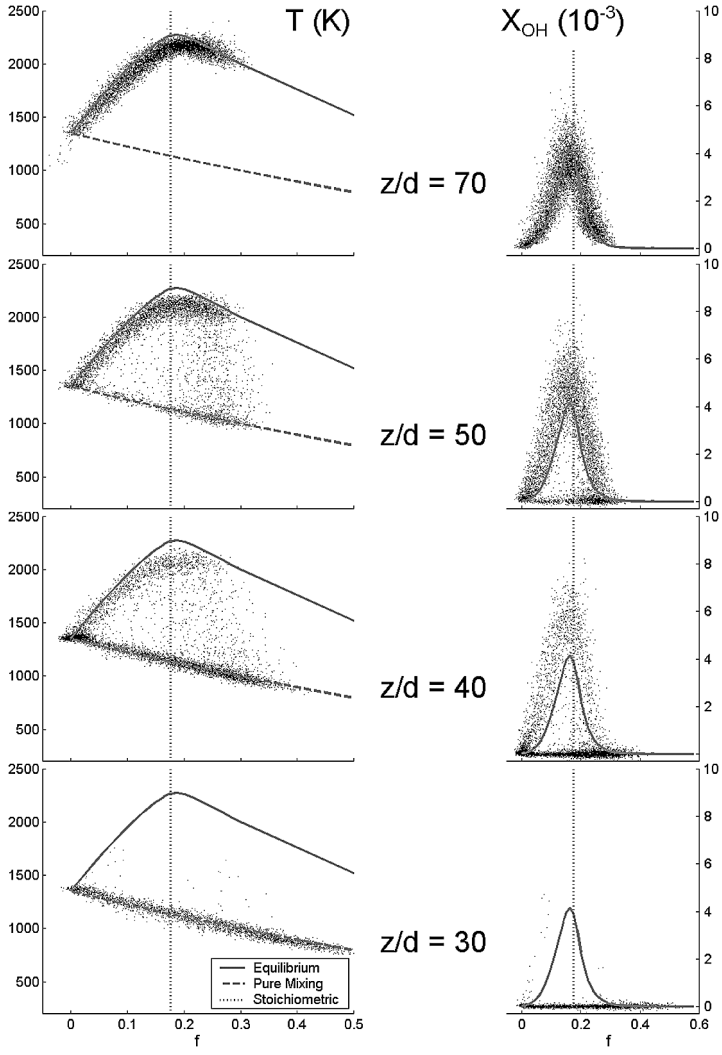

Fig. 3. Distributions of instantaneous temperature and OH mole fraction at four axial stations in the lifted CH_4/air flame.

case (Fig. 3) are distinctly bimodal, with the vast majority of temperature samples lying close to the mixing or equilibrium limits. For mixture fraction conditions below 0.2 (lean and near stoichiometric) there are very few samples within the interior, partially reacted part of the distribution. In contrast, at $z/d = 11$ in the H_2/N_2 flame (Fig. 4) the measured temperature samples are spread throughout the partially reacted interior region of the distribution, even for fuel-lean conditions.

It is expected that some of the partially reacted samples are experimental artifacts resulting from spatial averaging when the laser probe volume intersects a thin, partially premixed reaction zone at the leading edge of the lifted flame. The probability of such events depends on the PDF of flame position, the thickness of the reaction zone, and the size of the probe volume. In the case of the methane flame there is evidence of reaction already at $z/d = 30$ and there are still numerous samples on the pure mixing line at $z/d = 50$. Hence, the lifted flame base fluctuates over a vertical distance of many times the nozzle diameter, d, and most measurement samples are expected to miss the instantaneous flame base. The H_2/N_2 flame stabilizes much closer to the nozzle, with $H_{H_2}/d \approx 10$ compared to $H_{CH_4}/d \approx 35$. The fluctuations in the flame liftoff height are proportionally smaller for the hydrogen flame. The transition from the pure mixing line to the fully burning condition takes only about 6 diameters in the hydrogen flame ($8 < z/d < 14$). This corresponds to a higher probability that the transient reaction zone will intersect the probe volume. However, the distributions of temperature and Y_{OH} at $z/d = 11$ in the H_2/N_2

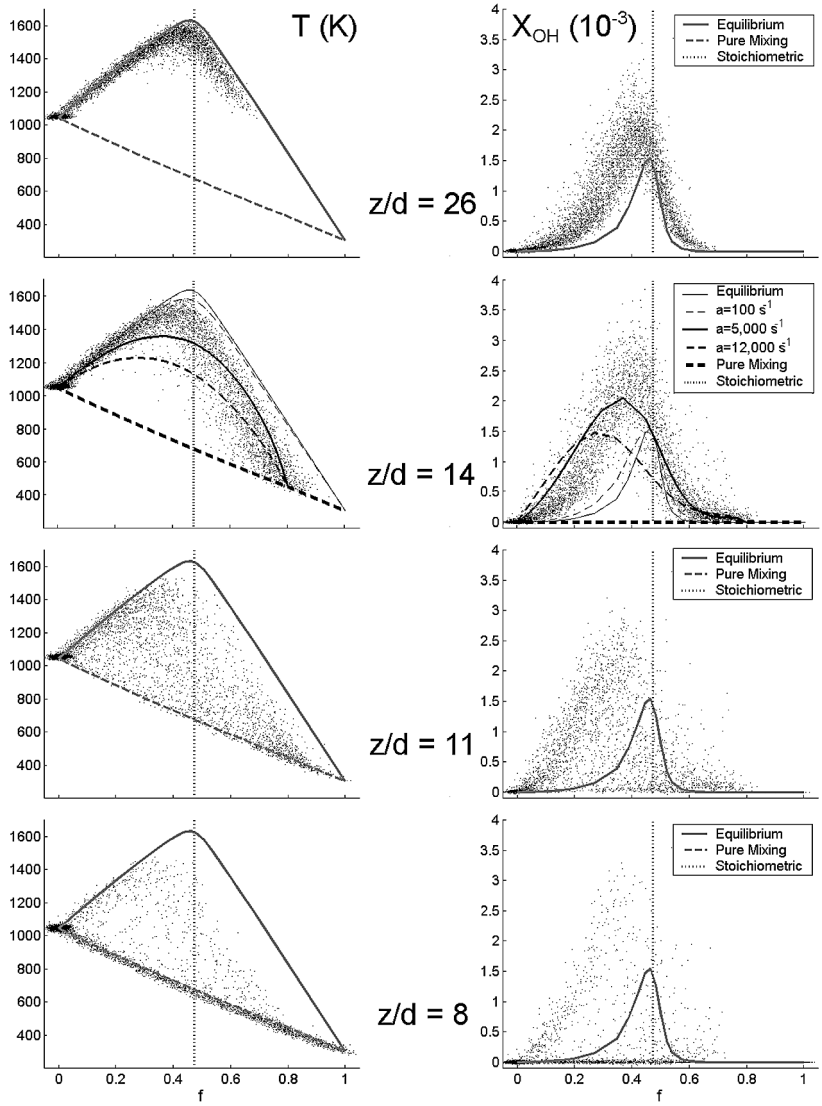

Fig. 4. Distributions of instantaneous temperature and OH mole fraction at four axial stations in the lifted H_2/N_2 flame [1].

flame cannot be attributed to spatial averaging effects if the reaction zone is thin. The absence of a bimodal distribution points to a distributed reaction zone or autoignition kernels or a combination of these phenomena, as discussed in our previous paper [1]. Autoignition may also be important in the lifted CH_4/air, as discussed below. Nonetheless, the qualitative differences between Figs. 3 and 4 suggest that there may be differences in the structure and stabilization mechanisms for these two flames. The differences cannot be conclusively determined from the single-point measurements alone, and future planar images of scalars and velocities would be useful in illuminating the nature of differences.

4. Combustion models

4.1. PDF model calculations

The flow field was computed using a standard k–ε model suitable for parabolic flows [7]. The joint-scalar PDF approach was used to model the turbulence–chemistry interactions. This approach was implemented in a parabolic marching scheme. Consequently, there is no mechanism for upstream propagation of a turbulent edge flame, and autoignition is the only possible mechanism for flame stabilization within this calculation. Several mixing models were incorporated into the joint-scalar PDF approach to model the lifted CH_4/air jet flame under the base

condition described above. These mixing models included the modified Curl mixing model [7], the Interaction by Exchange with the Mean [12], the Euclidean Minimum Spanning Tree mixing model [11], and the one-dimensional (1-D) mixing model [23] which resembles the Linear Eddy model [24] without stirring. In addition, the well-mixed reactor (Well-Mixed) is also included to represent the limit of infinitely fast mixing within each computational cell.

The radial distribution of velocity at $z/d = 0$ was approximated as uniform in the coflow ($r > d/2$), and as a fully developed turbulent pipe flow at the nozzle exit ($r \leqslant d/2$). The initial temperature and composition distributions were step functions across the nozzle inlet diameter of $d = 4.57$ mm. Initial concentrations of the major species and OH in the coflow were assigned the values measured at $z/d = 1$. The equilibrium concentrations of minor species were used for those species not measured. The equilibrium concentrations are determined from the measured coflow equivalence ratio and temperature listed in Table 1.

Other details of the numerical model are given as follows. The axial domain extended from $z/d = 0$ to 80, while the radial domain grew as z/d increased. A total of 70 grid cells was used in the radial domain. The Eulerian Monte Carlo PDF used 400 stochastic particles per grid cell. The local mixing frequency was modeled by the ratio of turbulent time scale to the scalar mixing time with a model constant set initially to the "standard" value of 2. For the present reacting flows the model constant was adjusted for each mixing model to achieve the best centerline distribution of both the Favre average and the variance of the mixture fraction. The resulting model constant value of 3 was found optimal for all mixing models except for the EMST model, where a value of 2 was found to give the best agreement with the experimental results.

There is little, if any, offset error in finding the location where light emerges from a flame front. The peak of maximum heat release rate and the peak of light emitting species, such as CH, C_2, or CO_2^*, are within a millimeter of each other, which is small systematic error compared to our measurement. The concentrations of the C_2H_4 and C_2H_2 intermediate species were used in combination to determine the flame liftoff height from the PDF calculations. This is based on the results from autoignition calculations showing that the time at peak heat release is bracketed by the times at peaks of C_2H_4 and C_2H_2. The axial locations where the mole fraction of C_2H_4 reached 100 ppm and C_2H_2 reached 2 ppm were recorded, and the liftoff height was then estimated as the average of the two axial values. This procedure is convenient (as the two species are in the reduced chemistry described below) and yields good agreement between the computationally determined liftoff height, when using the modified Curl model, and the experimentally determined one for the base-case flame.

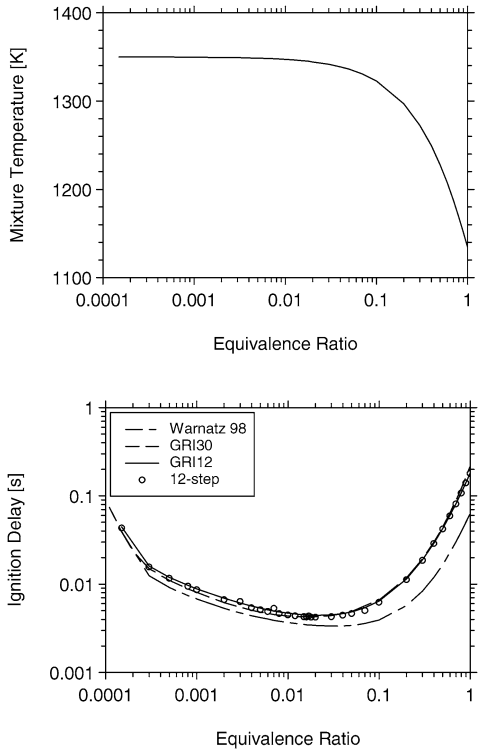

Fig. 5. Computed temperature (upper graph) versus equivalence ratio for mixing (without reaction) of the fuel and coflow. Comparison of computed ignition delays (lower graph) with different detailed mechanisms and the 12-step reduced chemistry.

4.2. Combustion chemistry

The present work implemented a 12-step reduced chemical kinetic mechanism developed from the GRI1.2 mechanism for methane combustion [25] that was optimized with various flame features including autoignition delay times for very lean mixtures. Due to the significance of autoignition in the present context, it is important to confirm that this reduced mechanism accurately reproduces the ignition delay times predicted by the original detailed mechanism. The mixture temperatures resulting from pure mixing of the fuel jet and the vitiated coflow are presented in the upper plot of Fig. 5 and show a decreasing trend with equivalence ratio. The lower plot of Fig. 5 presents a comparison of predicted ignition delays with GRI1.2 and GRI3.0 mechanisms, the 12-step reduced chemistry, and a high-temperature methane mechanism by Warnatz [26]. Because ignition delay depends strongly on temperature, the minimum ignition delay occurs in very lean mixtures. With both

GRI mechanisms and the 12-step reduced chemistry, the minimum delay occurs at an equivalence ratio around 0.02, which corresponds to ∼0.004 in mixture fraction. The overall performance of the 12-step chemistry is quite satisfactory. In comparison to the results from GRI mechanisms, the detailed mechanism by Warnatz predicts shorter ignition delays and the location of minimum delay is higher at 0.04. The differences are about 20% at the minimum locations and as large as a factor of 2 near the stoichiometric condition. The sensitivity of predicted ignition delays to chemistry model should be considered when comparing model predictions with experimental data.

5. Evaluation of mixing models

PDF calculations were carried out for the base-case condition using each of the five mixing models (M-Curl, IEM, EMST, 1-D, and Well-Mixed). Results from these calculations are compared below with each other and with experimental results for centerline profiles of selected scalars, scatter plots of temperature, and radial profiles of mixture fraction and temperature, and conditional statistics (mean and rms) of temperature and the mass fractions Y_{O_2} and Y_{OH}.

5.1. Centerline profiles

Centerline profiles provide information on the evolution of the flow that can be used to validate the PDF mixing models. Fig. 6 presents the centerline profiles of Favre-averaged mixture fraction and its fluctuation, temperature and its fluctuation, and mass fractions of O_2 and OH. The figure includes both experimental and computational results. All model results predict a flow with two stages. The initial stage, up to $z/d \sim 25$, involves mixing without reaction between the fuel jet and the vitiated coflow. This initial mixing stage is characterized by a slow temperature rise with relatively low levels of temperature fluctuation and negligible OH mass fraction. This is followed by a broad flame stabilization region characterized by a rapid temperature rise, larger temperature fluctuations, and the rise of Y_{OH}.

All model results produce the qualitative characteristics of the experimental centerline profiles. These include a moderate temperature increase due to mixing followed by a rapid temperature increase due to combustion; similar levels for the peak fluctuations of mixture fraction and temperature; slow oxygen dilution in the central jet due to entrainment of the coflow products, followed by rapid consumption of oxygen due to combustion; and similar OH concentration values downstream in the flame.

As noted earlier, the mixing model constants were adjusted such that the predicted peak fluctuation in mixture fraction was about the same for all models. Under this constraint, the EMST model gives a slightly slow decay of mixture fraction in the near field, in comparison to other models and the measurements, but it predicts reasonable fluctuations in mixture fraction and temperature. The predicted temperature rise along the jet centerline gives an indirect indication of the flame liftoff height because the centerline temperature rise will occur downstream of the flame stabilization zone. Among the different mixing models, the 1-D model predicts the centerline temperature rise closest to the nozzle exit followed by the Well-Mixed model, the EMST, the IEM, and the M-Curl model. This trend seems to correlate with the degree of randomness in mixing allowed in each model. In turbulent flows, fluid samples with different properties are brought together by convection and mixed via molecular diffusion. In the 1-D model mixing is achieved via diffusion between fluid parcels that lie in close proximity to each other in mixture fraction space. This local treatment tends to inhibit the mixing of parcels with substantially different compositions. For particles that are near the condition of minimum ignition delay, this localness in mixing could serve extended residence times at conditions conducive to autoignition, and this may result in the observed stabilization relatively close to the nozzle.

In contrast to the 1-D model, the M-Curl model picks randomly pairs of particles to mix. Thus fluid samples with vastly different properties can be mixed, and this apparently delays the stabilization of the flame by the process of autoignition. The EMST model ensures that mixing takes place with the localness property which may allow autoignition to occur earlier than with the M-Curl model under the present flame conditions. For brevity and because the models are not commonly used in combustion calculations, further details of the results from Well-Mixed and 1-D mixing models will not be presented.

5.2. Scatter plots of temperature versus mixture fraction

The predicted scatter plots of temperature versus mixture fraction obtained at different axial locations provide further metrics for model evaluation. Results from the remaining three mixing models (IEM, EMST, M-Curl) are contrasted in Fig. 7. Results from the IEM and EMST models are presented in the left and center columns, respectively, for axial locations $z/d = 25$, 30, 40, and 50. Distributions computed using the M-Curl model are plotted in the right-most column for axial locations $z/d = 30$, 40, 50, and 70. The choice of different axial stations to be plot-

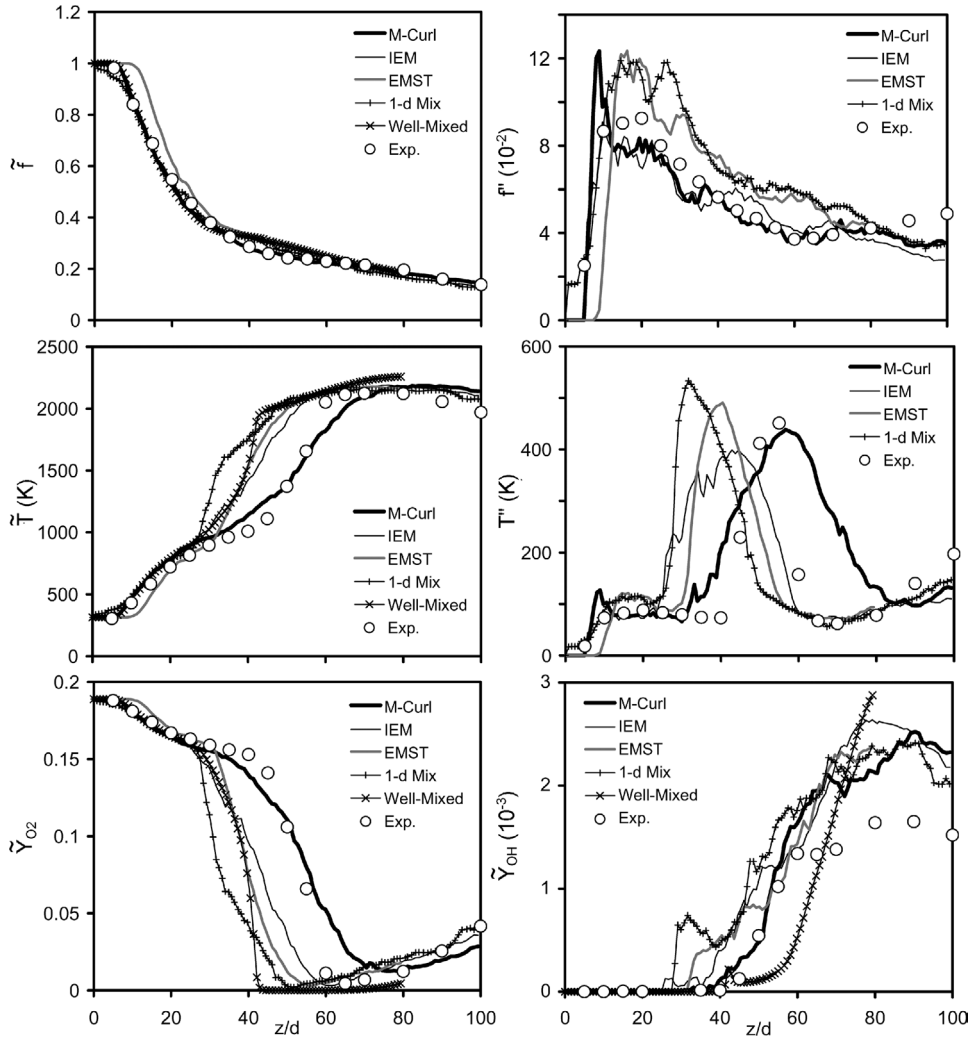

Fig. 6. Comparison of centerline profiles of Favre-averaged temperature and species mass fractions. Numerical PDF results: Modified Curl (M-Curl), Interaction by Exchange with the Mean (IEM), Euclidean Minimum Spanning Tree (EMST), one-dimensional diffusion (1-D Mix), and the perfectly mixed cells (Well-Mixed). Experimental results (Exp).

ted is due to the fact that the M-Curl model predicts a greater liftoff height. The locations are chosen to have similar states in terms of combustion progress. Also plotted are lines for adiabatic equilibrium and for mixing without reaction.

The scatter plots of temperature versus mixture fraction from the three PDF calculations are consistent with each model's treatment of mixing. The M-Curl model results exhibit a bimodal distribution filled with some intermediate states as a result of the mixing of randomly selected pairings. The IEM model results are clustered around two bands with few points scattered in between. The points in the lower band gradually react to reach the fully burnt temperatures at the lower axial locations ($z/d = 30$ and 40). Pure mixing at the lower locations is not well represented by the IEM model. The EMST model results exhibit a low-variance distribution consistent with a model that is local in composition space. Since a short liftoff height is predicted, the pure mixing on the fuel lean side at $z/d = 25$ is not captured. However, the EMST model does reasonably predict flame broadening at $z/d = 25$. The broad distributions predicted with the M-Curl and EMST mixing models are most consistent with the experimental results even though the scatter in the experimental results is due, in part, to experimental uncertainty.

5.3. Radial profiles and conditional statistics

Fig. 8 shows radial profiles of Favre-averaged mixture fraction and temperature from the measure-

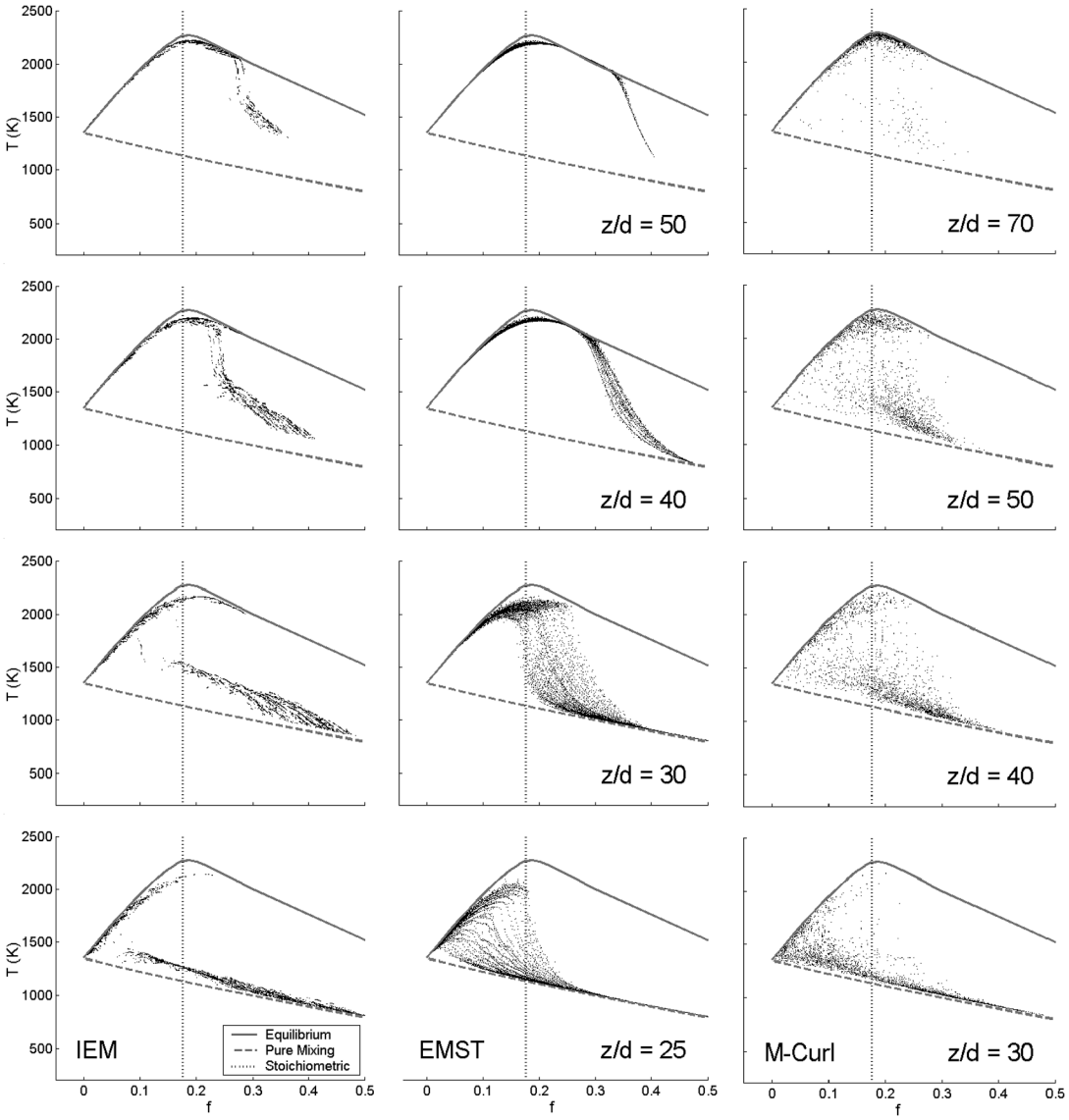

Fig. 7. Scatter plots of temperature versus mixture fraction with increased axial distance for IEM and EMST model results at $z/d = 25$, 30, 40, 50, and for M-Curl model results at $z/d = 30$, 40, 50, and 70. Also plotted are adiabatic equilibrium values (solid line) and nonreacting (dashed line; pure mixing) conditions. The vertical dotted line indicates the stoichiometric condition.

ments and from PDF calculations using the modified Curl mixing model. The outer end of each measured profile up to $z/d = 50$ reaches the undiluted coflow condition and shows near-zero temperature fluctuation. Thus, the experimental jet is isolated from the ambient air by the hot coflow for a distance of at least $z/d = 50$. The elevated temperature fluctuations at the outer edge of the temperature profile at $z/d = 70$ indicate some degree of mixing of ambient air. However, as noted previously, the temperature scatter data from this streamwise location (Fig. 3) show only a very small number of points that correspond to such mixing. Thus, penetration of ambient air into the measurement region is rare even at $z/d = 70$.

The radial profiles for temperature in Fig. 8 indicate no reaction in the first 30 diameters from the exit nozzle. Initially, mixing without reaction occurs between the vitiated coflow and fuel jet. It is not until $z/d = 40$ that we see a distinct increase in the temperature fluctuations and a rise in the mean temperature above the coflow condition. These measurements are consistent with visually observed liftoff height being near $z/d = 35$. Agreement between measured and modeled profiles of mixture fraction and

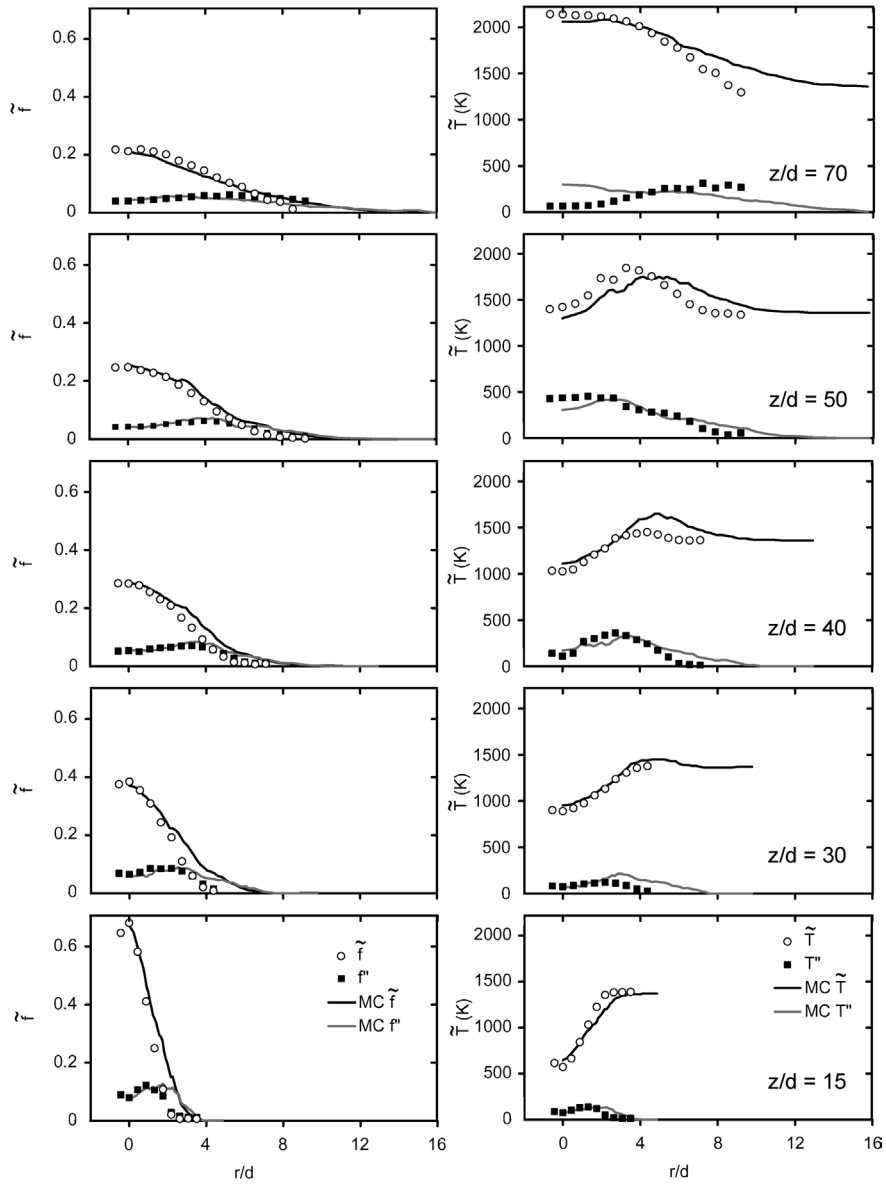

Fig. 8. Radial profiles of Favre-averaged mixture fraction and temperature with increased axial distance. Plotted are experimental results (symbols) and PDF with M-Curl mixing results (lines).

its fluctuation is reasonably good, although the model predicts somewhat broader profiles. The broader predicted mixture fraction profiles correspond to an outward shift in the predicted peak temperature relative to the measurements at $z/d = 40$ and $z/d = 50$. At $z/d = 70$, the measured mean temperature and its rms at the outer edge of the profile show the effects of mixing with air since the mean temperature falls below that of coflow. Near the jet centerline, the rms values predicted by the M-Curl mixing model are seen to exceed the data. The measured mean temperature reaches its maximum at the centerline ($\tilde{f}$ about 0.2) and the corresponding scatter data show that the flame is fully burning. Consequently, T'' is expected to be lower than those at other locations. The M-Curl results still show some unburnt samples at $z/d = 70$ (Fig. 7), and hence the predicted T'' is higher than data.

Results for the conditional ensemble average and rms fluctuation of temperature, Y_{O_2}, and Y_{OH} are shown in Figs. 9–11, where computations using the M-Curl model (lines) are compared to the experiment (symbols). These conditional statistics are complementary to the scatter plots (Figs. 3 and 7) in pro-

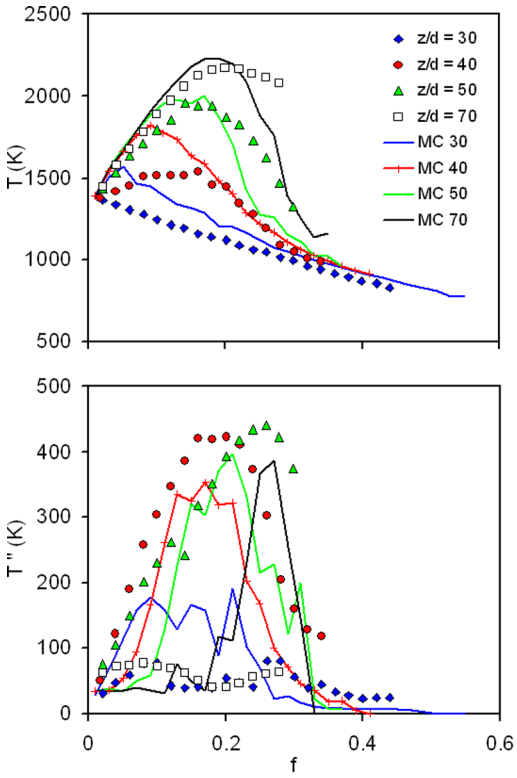

Fig. 9. Evolution of the conditional ensemble average and rms fluctuation of temperature. Plotted are experimental results (symbols) and PDF with M-Curl mixing results (lines).

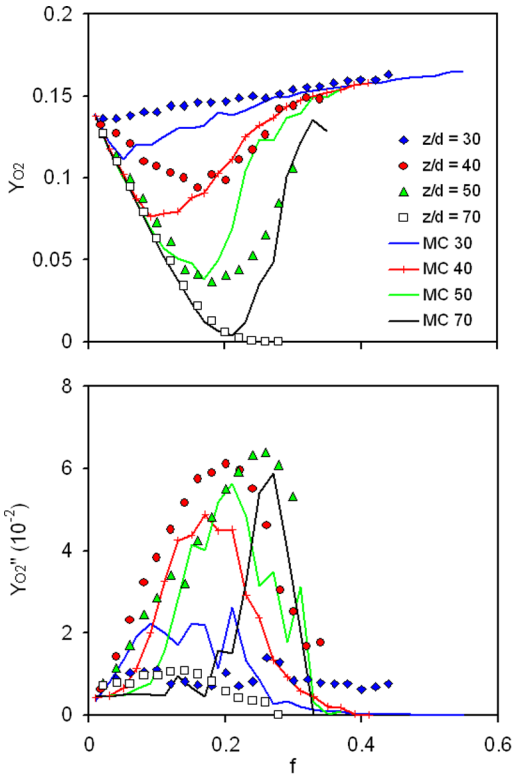

Fig. 10. Evolution of the conditional ensemble average and rms fluctuation of O_2 mass fraction. Plotted are experimental results (symbols) and PDF with M-Curl mixing results (lines).

viding insights on the scalar structure and evolution the lifted CH_4/air jet flame, as well as highlighting the similarities and differences between measured and calculated results. Considering the conditional averages first (top figures in Figs. 9–11), it is apparent that the PDF results for temperature and Y_{O_2} at very lean conditions tend to follow a trajectory close to the fully reacted (equilibrium) line before deviating and cutting across the interior, partially reacted portion of the domain. Recall from the discussion of Fig. 5 that the minimum ignition delay occurs in very lean mixtures near $f = 0.004$. Therefore, flame stabilization within the calculation occurs by autoignition of these very lean samples followed by mixing a subsequent reaction at other mixture fraction values. Note that this preference for reaction in very lean mixtures is more obvious in the scatter plots for the IEM and EMST calculations in Fig. 7. From Fig. 3 we know that the scatter data from measurements of lean samples at $z/d = 30$ in the flame stabilization region are more obviously bimodal, with many lean samples remaining near the pure-mixing line. The corresponding conditional mean curve for $z/d = 40$ in Figs. 9–11 exhibits a broad peak with the fuel-lean portion being roughly halfway between the mixing-only and fully reacted limits. Farther downstream, at $z/d = 50$, the majority of samples with fuel-lean mixture fractions are close to the fully reacted curve. Generally, the conditional mean results from the PDF model are suggestive of a process that begins at fuel-lean conditions and then extends toward stoichiometric and then fuel-rich conditions as streamwise distance increases.

With regard to the conditional fluctuations (bottom figures in Figs. 9–11) consider that maximum possible rms levels for temperature and Y_{O_2} at a given mixture fraction correspond to distributions that are perfectly bimodal, with half the samples on the pure mixing line and half on the equilibrium curve or, alternatively, a curve representing the reacted samples at each downstream location. Lower rms values occur when there is a distribution of partially reacted samples in between these limits, and the conditional rms becomes small when all samples at a given mixture fraction are either at the pure-mixing limit or near the same reacted state. The measured conditional fluctuations at $z/d = 40$ and 50 are roughly 450 K, while the upper limit for a distribution between the mixing line and the reacted state is roughly 600 K. Based on the measured conditional means in Figs. 9–11, measure-

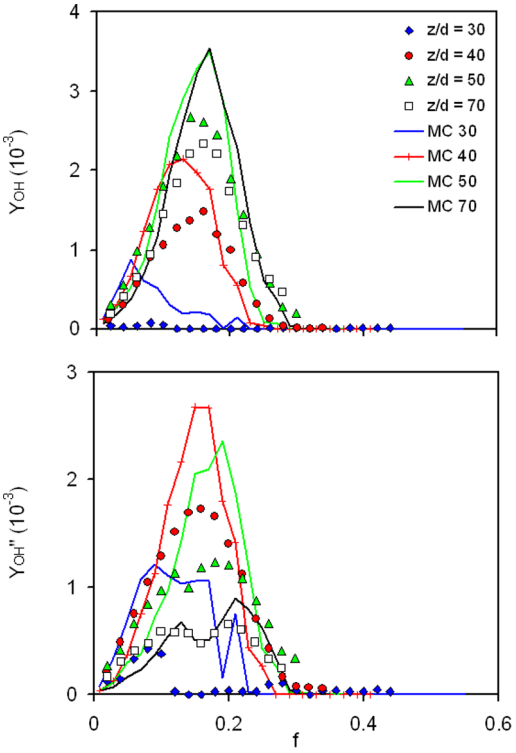

Fig. 11. Evolution of the conditional ensemble average and rms fluctuation of OH mass fraction. Plotted are experimental results (symbols) and PDF with M-Curl mixing results (lines).

ments at the average liftoff height of $z/d = 35$ should yield conditional mean temperatures near the stoichiometric condition that are approximately halfway between the mixing and the reacted state. Due to the strongly bimodal character of the measured scatter data, we would expect the corresponding conditional rms temperature fluctuations to be even closer to the theoretical upper limit.

The conditional rms results from the PDF calculation show that the peaks in the fluctuations of T and Y_{O_2} are somewhat below the experimental results. This appears to be associated with the fact that the prediction shows a significant population of scalar states that have moved slightly away from the mixing line (e.g., M-Curl results in Fig. 7 at $z/d = 40$), whereas the measurements show the comparable population staying on the mixing line (within the experimental uncertainty). In Figs. 9 and 10 the predicted curves for fluctuations of T and Y_{O_2} are also observed to shift to larger mixture fraction values as we move downstream. This trend is consistent with a flame stabilization process that begins at very lean conditions, which correspond to the minimum ignition delay times, and then progresses toward richer mixtures. The experiment shows a similar trend for data from the stabilization region ($z/d = 40$ and $z/d = 50$). However, the experimental trend ends before $z/d = 70$ because the riches samples are already near the fully reacted limit.

6. Liftoff height sensitivity

The sensitivity of the flame liftoff height to jet velocity, coflow velocity, and coflow temperature was examined by parametric variation, both computationally and experimentally. In the parametric experiments the liftoff height was determined by digital imaging of the luminous flame base. The vitiated coflow temperature under different flow conditions was determined by thermocouple measurements. Computations were carried out using the M-Curl model, since it best predicted the base case.

As was shown in Figs. 3 and 7, all chemical kinetic activity occurs in regions of the flow with a low mixture fraction ($f < 0.4$) that are also associated with lower velocities, lower turbulence intensities, and higher temperatures. As such, the combustion processes of the lifted jet flame should be more sensitive to coflow conditions than jet conditions. This is indeed the case shown in Figs. 12 and 13, where the sensitivity of liftoff height to jet exit velocity and coflow velocity is examined. It should be noted that the two figures are based on the same dataset; in each case the liftoff height is plotted against one of the two velocities (jet/coflow) using the other velocity as a parameter (coflow/jet). A comparison of the two figures makes it apparent that the liftoff height is very sensitive to the coflow velocity. The sensitivity of liftoff height to coflow velocity was also investigated by Dahm and Dibble [27], who considered lifted flames in unheated air and developed a model predicting the strong sensitivity of flame blowoff to coflow velocity.

Kalghatgi [28] proposed a liftoff height correlation in terms of the maximum laminar flame speed, coflow density, and jet properties including velocity, viscosity, and density:

$$H_K = 50\left(\frac{\nu_{\text{jet}} V_{\text{jet}}}{S_{L,\max}^2}\right)\left(\frac{\rho_{\text{jet}}}{\rho_{\text{coflow}}}\right)^{1.5}. \tag{11}$$

This correlation was developed using scaling arguments for the case of fuel jets into quiescent air (i.e., no coflow). Perhaps fortuitously, the correlation accurately predicted the liftoff height for the H_2/N_2 jet flame ($H_K/d = 11.4$, $H_{\text{exp}}/d \approx 10$) previously presented [1]. In contrast, the CH_4/air results plotted in Fig. 12a show large discrepancies between Kalghatgi's model and the experimental data.

The PDF model with the M-Curl mixing model predicts the approximately linear sensitivity of liftoff

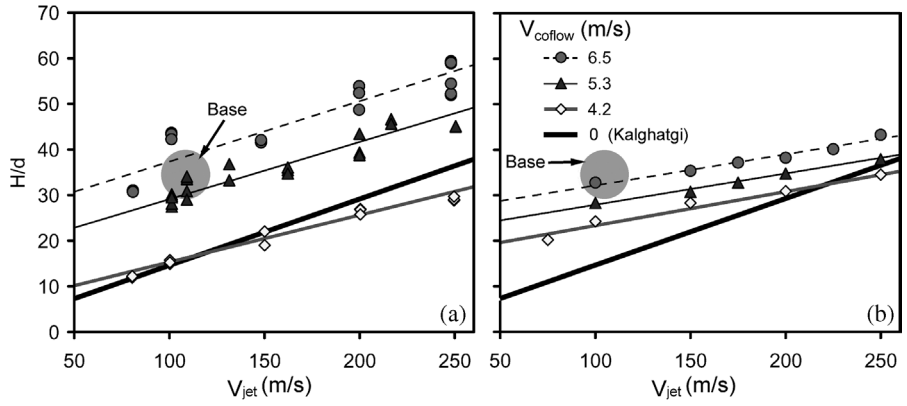

Fig. 12. Sensitivity of CH_4/air flame liftoff height to jet exit velocity, with coflow velocity as a parameter. The shaded circle represents the base-case liftoff height established by the unaided eye. Plotted are the experimental results (a) and the PDF with M-Curl mixing results (b). The thick line shows the prediction from Kalghatgi's correlation.

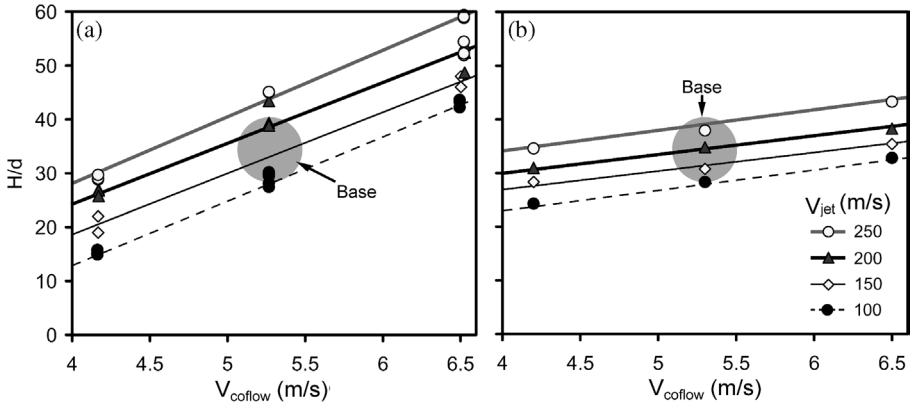

Fig. 13. Sensitivity of CH_4/air flame liftoff height to coflow velocity, with jet exit velocity as a parameter. The shaded circle represents the base-case liftoff height established by the unaided eye. Plotted are the experimental results (a) and the PDF with M-Curl mixing results (b). (The same data as in Fig. 12 are used here.)

height to jet velocity reasonably well, as can be seen by comparing the slopes of the experimental and computational results in Fig. 12. However, the model underpredicts the sensitivity of liftoff height to coflow velocity, as can be seen in Fig. 13, where the lines showing the measured trend (Fig. 13a) have clearly a steeper slope than the corresponding lines for the modeled trend (Fig. 13b). This underprediction may be due to assumptions inherent in the k–ε turbulence model, mixing model, inlet conditions, or parabolic flow assumption, and further work will be required to identify the reasons for this difference between measured and modeled results.

The sensitivity of liftoff height to coflow scalar conditions was investigated by varying the equivalence ratio of the premixed flames that form the vitiated coflow. Changing the equivalence ratio also changes the concentrations of oxygen and radicals in the coflow. However, since reaction rates are exponentially dependent on temperature, while they are only linearly dependent on composition, the combustion processes are most sensitive to temperature. As shown in Fig. 14, the sensitivity of liftoff height to coflow temperature is strong and approximately linear over the range of conditions considered. A 5% drop in coflow temperature (60 K) roughly doubles the liftoff height. While the PDF method with M-Curl mixing model predicts this temperature sensitivity relatively well, Kalghatgi's model significantly underpredicts the sensitivity to temperature. The PDF modeling with well-mixed cells was also tested and is shown in Fig. 14 to do a reasonable job of predicting the relative change in liftoff height (also nearly doubling with a 60 K decrease), even though the liftoff heights are themselves under predicted. The reasonable approximation by the fast and inexpensive well-mixed combustion model suggests that the sensitivity of liftoff height to temperature can be captured simply

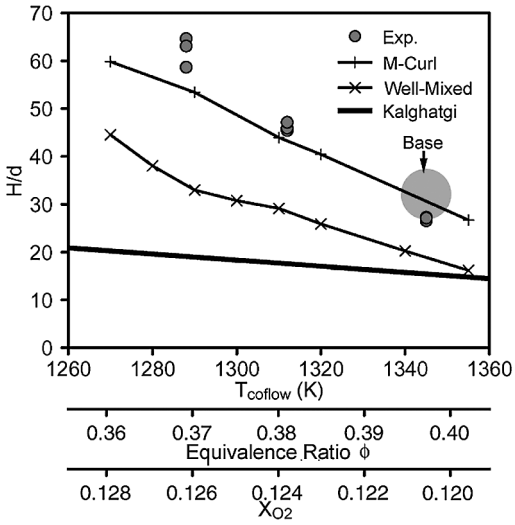

Fig. 14. Sensitivity of liftoff height to measured coflow temperature and equivalence ratio. The shaded circle represents the base-case condition. Plotted are the experimental results, PDF with M-Curl mixing results, PDF with well-mixed cells results, and Kalghatgi's model. The bottom abscissas show the variation in ϕ and oxygen level that resulted in the coflow temperature variation.

by employing the proper chemical kinetics submodel. Therefore, details of molecular mixing may not be important in determining this sensitivity.

An important result from this parametric study is that PDF calculations using the modified-Curl mixing model within a parabolic marching approach, which relies on autoignition for initial flame stabilization, do a reasonably good job of predicting the effects of changing coflow conditions on the measured liftoff height. This might be interpreted as an indication that autoignition is the controlling mechanism for stabilization of these lifted flames in vitiated coflow. However, there is other evidence to suggest that turbulent edge flame propagation may be an important mechanism in the laboratory flame. Specifically, the computed scatter data for temperature show that reaction is initiated in very lean mixtures (shortest ignition delay) and progressively spreads to higher mixture fractions. The experimental scatter data, although limited with respect to the number of measured locations, do not show such a preference for reactivity at very lean reactions. The maximum premixed laminar flame speed for reactant conditions along the mixing line is about 3.2 m/s and occurs on the slightly lean side of the stoichiometric mixture fraction, and this may be sufficient to support stabilization by edge flame propagation. Additional experiments beyond the present multiscalar point measurements are needed before we can fully understand the relative importance of autoignition and turbulent edge flame propagation in stabilizing these lifted CH_4/air flames in vitiated coflow.

7. Conclusions

Experimental and numerical results on lifted flames in a hot (vitiated) coflow were presented. Laser-based multiscalar point measurements provided a detailed dataset for a base-case condition of a lifted CH_4/air turbulent jet flame in a vitiated coflow of H_2/air combustion products. Complementing this base case, a series of parametric experiments provided information on sensitivity of the liftoff height to the jet velocity, coflow velocity, and coflow temperature. Probability density function combustion models, each employing a different molecular mixing submodel, were tested for their capacity to capture the features of the base-case flame. Each of the mixing models, modified Curl, Euclidean Minimum Spanning Tree, and IEM, yielded predictions of stable lifted flames and reasonably predicted some qualitative features of the base-case condition.

The behavior of the PDF combustion model with M-Curl mixing model was further tested by comparison with experimental results on the relative sensitivity of liftoff height to the jet velocity, coflow velocity, and coflow temperature. The model predicted the sensitivity to jet velocity and coflow temperature reasonably well. However, the sensitivity to the coflow velocity was underpredicted. The liftoff height exhibited the highest sensitivity to coflow temperature.

In the evaluation of the PDF mixing models, the most compelling argument in favor of the M-Curl and EMST mixing models was the appearance of the scattered data of temperature versus mixture fraction. The data showed an evolution from a pure mixing (nonreacting) condition to a reacting condition. At the flame base, the scatter data distribution was broad and bimodal, consistent with a relatively thin turbulent reaction zone fluctuating around a laser probe volume. An important difference between modeled and measured results was that the scatter data from the PDF calculations showed clear indications of a flame stabilization process that initiates with autoignition in very lean mixtures, whereas the measurements do not show any obvious indication that very lean samples react first. Further work will be needed before firm conclusions may be drawn regarding the relative importance of autoignition and turbulent edge flame propagation as stabilization mechanisms for these lifted flames.

These methane flames exhibit characteristics different from the previously reported H_2/N_2 lifted flame, particularly with regard to the distributions of scatter data for reactive scalars in the stabilization region. Calculations of both of these flames using

models that allow for both autoignition and upstream flame propagation should yield interesting insights on the flame stabilization mechanisms for fuel flows injected into high-temperature environments.

Acknowledgments

Research at UC Berkeley was supported by NASA Glenn Research Center, under Contract NAG3-2103. Experiments conducted at Sandia were supported by the United States Department of Energy, Office of Basic Energy Sciences.

References

[1] R. Cabra, T. Myhrvold, J.-Y. Chen, R.W. Dibble, A.N. Karpetis, R.S. Barlow, Proc. Combust. Inst. 29 (2002) 1881–1888.
[2] A.R. Masri, R. Cao, S.B. Pope, G.M. Goldin, Combust. Theory Model. 8 (2004) 1–22.
[3] G.M. Goldin, AIAA 2005-555 (2005).
[4] R. Cao, S.B. Pope, A.R. Masri, Combust. Flame 142 (2005) 438–453.
[5] S.B. Pope, Proc. Combust. Inst. 23 (1990) 591–612.
[6] R.O. Fox, Computational Models for Turbulent Reacting Flows, Cambridge Series in Chemical Engineering, Cambridge Univ. Press, Cambridge, UK, 2003.
[7] J. Janicka, W. Kolbe, W.J. Kollmann, Non-Equil. Thermodyn. 4 (1979) 47–66.
[8] N.S.A. Smith, R.W. Bilger, C.D. Carter, R.S. Barlow, J.-Y. Chen, Combust. Sci. Technol. 105 (1995) 357–375.
[9] P.A. Nooren, H.A. Wouters, T.W.J. Peeters, D. Roekaerts, U. Maas, D. Schmidt, Combust. Theory Model. 1 (1997) 79–96.
[10] S. Subramaniam, S.B. Pope, Combust. Flame 117 (1999) 732–754.
[11] S. Subramaniam, S.B. Pope, Combust. Flame 115 (1998) 487–514.
[12] J. Villermaux, J.C. Devillon, in: Proceedings from the 2nd International Symposium on Chemical Reaction Engineering, Elsevier, New York, 1972, p. 13.
[13] Q. Tang, J. Xu, S.B. Pope, Proc. Combust. Inst. 28 (2000) 133–139.
[14] P.R. Lindstedt, S.A. Louloudi, E.M. Vaos, R.W. Bilger, Proc. Combust. Inst. 28 (2000) 149–156.
[15] R.S. Barlow, J.H. Frank, Proc. Combust. Inst. 27 (1998) 1087–1095.
[16] R.S. Barlow, G.J. Fiechtner, C.D. Carter, J.-Y. Chen, Combust. Flame 120 (2000) 549–569.
[17] Q.V. Nguyen, R.W. Dibble, C.D. Carter, G.J. Fiechtner, R.S. Barlow, Combust. Flame 105 (1996) 499–510.
[18] B.B. Dally, A.R. Masri, R.S. Barlow, G.J. Fiechtner, D.F. Fletcher, Proc. Combust. Inst. 26 (1996) 2191–2197.
[19] R.S. Barlow, A.N. Karpetis, J.H. Frank, J.-Y. Chen, Combust. Flame 127 (2001) 2102–2118.
[20] R.W. Bilger, S.H. Stårner, R.J. Kee, Combust. Flame 80 (1990) 135–149.
[21] T.S. Cheng, J.A. Wehrmeyer, R.W. Pitz, Combust. Flame 91 (1992) 323–345.
[22] A. Brockhinke, P. Andresen, K. Höinghaus, Appl. Phys. B 61 (1995) 533–545.
[23] D. Geyer, A. Dreizler, J. Janicka, A.D. Permana, J.-Y. Chen, Proc. Combust. Inst. 30 (2005) 711–718.
[24] A.R. Kerstein, J. Fluid Mech. 240 (1992) 289–313.
[25] C.J. Sung, C.K. Law, J.-Y. Chen, Combust. Sci. Technol. 156 (2000) 201–220.
[26] J. Warnatz, private communication (2000).
[27] W.J.A. Dahm, R.W. Dibble, Proc. Combust. Inst. 22 (1988) 801–808.
[28] G.T. Kalghatgi, Combust. Sci. Technol. 41 (1984) 17–29.